

# Residual stresses due to gas arc welding of aluminum alloy joints by numerical simulations

M. Ahmadzadeh · B. Farshi · H. R. Salimi ·  
A. Hoseini Fard

Received: 21 April 2011 / Accepted: 27 October 2011 / Published online: 15 November 2011  
© Springer-Verlag France 2011

**Abstract** This study deals with the numerical simulation of the gas arc welding process of Aluminum tee joints using finite element analysis and evaluation of the effect of welding parameters on residual stress build up. The 3D simulations are performed using ABAQUS code for thermo-mechanical analyses with moving heat source, material deposition, solid-liquid phase transition, temperature dependent material properties, metal elasticity and plasticity, and transient heat transfer. Quasi Newton method is used for the analysis routine and thermo-mechanical coupling is assumed; i.e. the thermal analysis is completed before performing a separate mechanical analysis based on the thermal history. The residual stress build up and temperature history state in a three-dimensional analysis of the tee joint is then compared to experimental results. Hole drilling method is used for measuring the residual stress, while temperature history is measured by thermocouples. After carrying out numerical simulations, the effects of voltage/current, welding speed, material thickness and size of electrode on residual stress build-up and resulting distortions are evaluated.

**Keywords** Finite element · Aluminum alloys · Residual stresses · Gas arc welding · Welding parameters

## Introduction

Welding is commonly used for permanently joining metals in the manufacturing industries. Highly non-uniform field temperature, phase transfer and plastic deformation produced during welding process give rise to residual stresses and distortions in the final product. Tensile residual stresses adversely influence fatigue, creep strength, stress corrosion cracking, brittle fracture and reduction of ultimate strength. Compressive residual stresses also adversely affect the behavior of metal products such as yield and buckling strength; Therefore prediction and control of residual stresses is important in the production of metal products.

The prediction of welding residual stresses has been studied by many researchers. Finite element analysis (FEA) has been the main tool used by several authors [1–4, 12–26] to perform welding simulations in order to predict welding residual stresses in different types of joints and materials. Main difficulty in prediction is the complex variations of temperature, thermal contraction, expansion and changes of material properties with time and space in the model. Furthermore, modeling of the welding process must be accounted for the specialized effects of the practical aspects of welding such as movement of welding arc, material deposition, and metallurgical transformations.

Oddy et al. [6] stated that prediction of the temperature field requires a nonlinear transient 3D analysis. Studies by Chao and Qi [5] concluded that 3D modeling of the welding process is essential for practical problems to provide accurate residual stress and distortion predictions that cannot be obtained from 2D simulations. McDill et al. [10] also stated that some 2D predictions of residual stresses for materials exhibiting phase transformations show large differences with experimental measurements, leading to their choice of a 3D finite element model. Due to the

---

M. Ahmadzadeh (✉) · B. Farshi  
Department of Mechanical Engineering,  
Iran University of Science & Technology,  
Narmak 16846, Tehran, Iran  
e-mail: Mohsen.ahmadzade@gmail.com

H. R. Salimi · A. Hoseini Fard  
Department of Marine Structures,  
Iran Air Naval Research Center,  
Chamran 7194915685, Shiraz, Iran

**Table 1** Chemical composition of aluminum alloys 2519-T87 and 2319 (mass%) [29]

Element	Zn	Fe	Si	Mg	Zr	Ag	V	Ti	Mn	Cu
Base metal (Aluminum alloy 2519-T87)	0.1	0.3	0.25	0.05–0.4	0.1–0.25	–	0.05–0.15	0.02–0.1	0.01–0.05	5.3–6.4
Filler metal (aluminum alloy 2319)	0.1	0.03	0.2	0.02–0.4	0.1–0.25	–	0.05–0.15	0.1–0.2	0.2–0.4	5.6–6.8

above prior conclusions, a 3D simulation model is also adopted in this research.

Most of the researchers have reported the coupling of thermal and structural model in their analysis procedures [2, 4–9, 13–16, 18–21], using the three dimensional double ellipsoid proposed by Goldak et al. [12] to model the heat source; Therefore in this study both the coupling method and double ellipsoid heat source are also employed.

Karlsson and Josefson [4] utilize the so-called element “birth” facility of ADINAT software to keep weld elements ahead of the welding arc inactive in the thermal analysis, until the front of the heat source reaches those elements. In the mechanical analysis reported in their research, the elements are kept inactive until the front of the source has passed the element by about an additional element length. In this study however, the elements are kept inactive by means of a subroutine, until the front of the source has passed the inactive element by three element length. Most of the researchers [4, 7, 11, 15, 23] have reported that the effect of radiation is typically much smaller than the effect of convection in the heat transfer, which is also followed herein.

The effects of some welding parameters on residual stresses have been studied by Ribycki et al. [27]; who studied the effect of wall thickness and pipe diameter using axisymmetric FEA model with lateral symmetry for multi-pass welding of stainless steel pipes. Dong et al. [3] used a shell model with lateral symmetry to inspect the effect of pipe wall thickness

and welding speed for pipes of various thicknesses. Fricke et al. [28] used a full 3D model for pipe welding and presented residual stresses on two different pipe diameters.

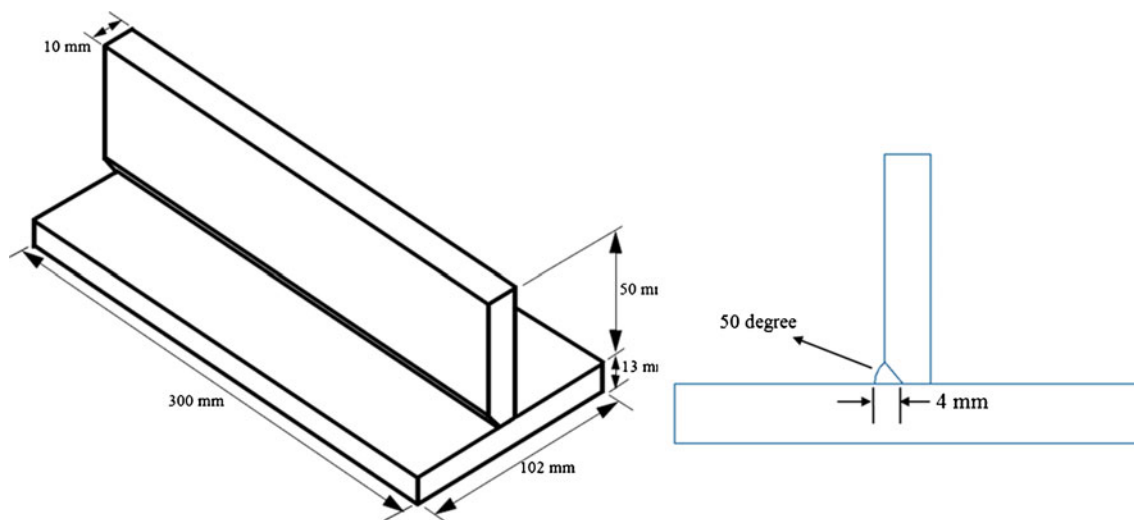
In this study the effects of voltage/current, speed of welding, thickness of welding pieces, and electrode sizes on residual stresses are also evaluated by finite element models. As Tee joint welding is widely used in different application fields such as buildings, bridges, aerospace structures and etc. it is also examined here.

### Experimental procedure

The base metal used in the experiments here is aluminum alloy 2519-T87 and the filler metal is aluminum alloy 2319. Table 1 contains the chemical compositions of both 2519 and 2319 aluminum alloys [29].

The designed process experiment is the welding of a tee joint with just one fillet weld on one side of the joint. The welding parameters are listed as below:

Current: 300–400A, voltage: 33–37 V and electrode speed: 6 mm/s. There was no pre or post-weld heat treatment and the welding process was performed in temperature of 27°C. By heating the plates to 250°C temperature and decreasing to ambient temperature very slowly Stress relief procedure was done on plates

**Fig. 1** Tee joint configuration

before welding. The dimensions and configuration of the tee joint are shown in Fig. 1. After welding, hole drilling method is to be adopted for measurement of the welding residual stresses, while the temperature history is to be monitored by thermocouples placed on the thin plate side that usually has the critical stresses. In these experiments, the strain gauges with designation of EA-XX-031RE-120 and .031 (IN) length are used.

Six strain gauges were used to measure the residual stresses and one thermocouple was used to monitor the temperature history, whose locations on the welded piece are shown in Fig. 2. The RS-200 Milling Guide was used for accurate positioning of the drilling bit for a hole through the center of the strain gauge rosette. The hole diameters were in range of 0.03 to 0.04 in, and the holes' depth was 0.03 in.

There was limitation in experiment method to set up the thermocouple near the melting zone due to high temperature [30]. Strain gauges are not mounted near the welding area due to restriction caused by tee joint shape for drilling holes near welding joint with RS-200 Milling Guide. The specified mechanical boundary conditions are those which are just sufficient to prevent rigid body motion of the model. Those are explained in boundary condition section in details.

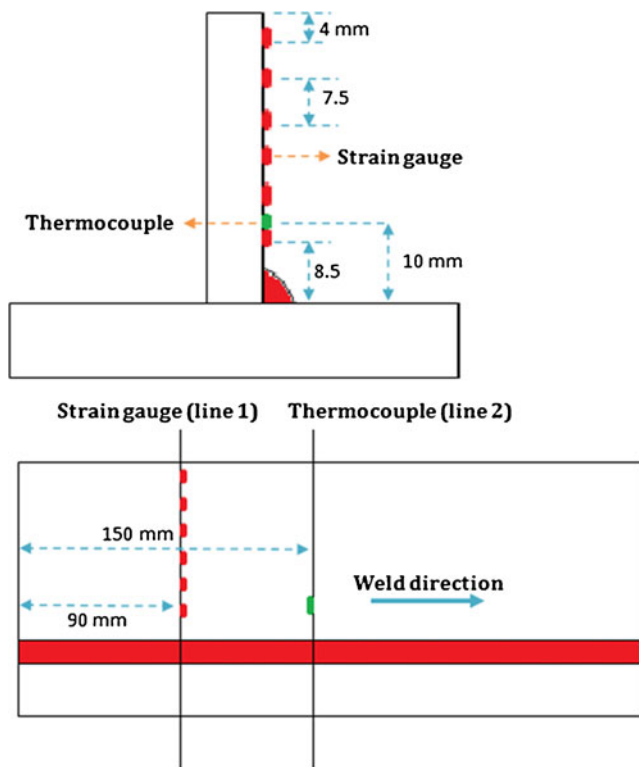


Fig. 2 Strain gauge and thermocouple positions on plate piece

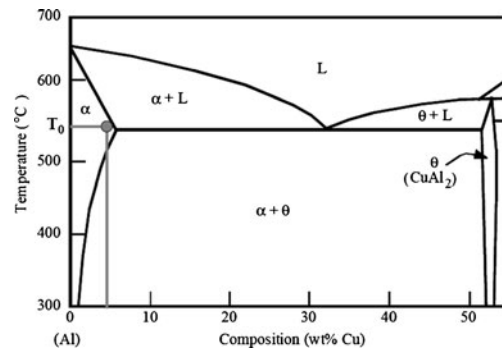


Fig. 3 Phase diagram of aluminum alloy 2519-T87 [29]

### Finite element modeling

#### Model geometry

Due to the wide spread use of tee joints in metal industries it is adopted in this research as the physical model. Overall dimensions of the 3D model of the experimental piece are shown in Fig. 1.

It's corrected that double side of welding modeled but elements of one side were just active during simulation. As stated earlier, a 3D modeling of the welding process is essential for practical problems as it can provide accurate residual stress and distortion results which cannot be obtained from 2D simulations. In 2D models transverse stresses and 3D effect of electrode movement are all neglected. The only problem of a 3D model analysis is its time consuming due to its domain size; which in this case it took about 19 h on a quad (four core) CPU with 4 Gigabyte RAM Pc to be run.

After evaluating the accuracy of finite element model and comparing it with experimental results, three models of connecting plates with different thicknesses were designed to study the effect of thickness variation. The choices of plate thicknesses were 12, 10, 8, mm.

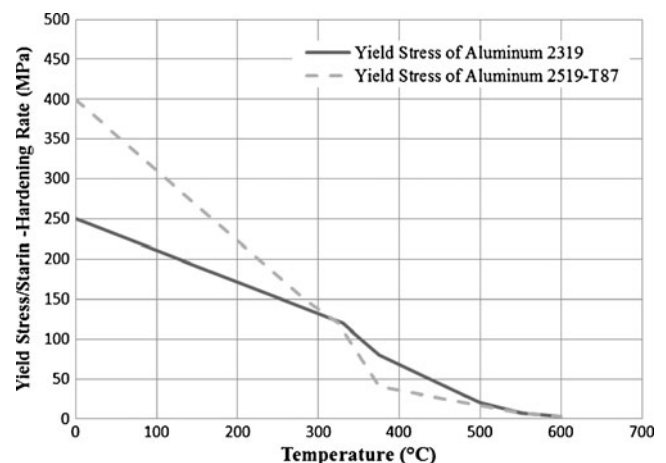


Fig. 4 Yield stress versus temperature for aluminum alloy 2519-T87 and 2319 [29]

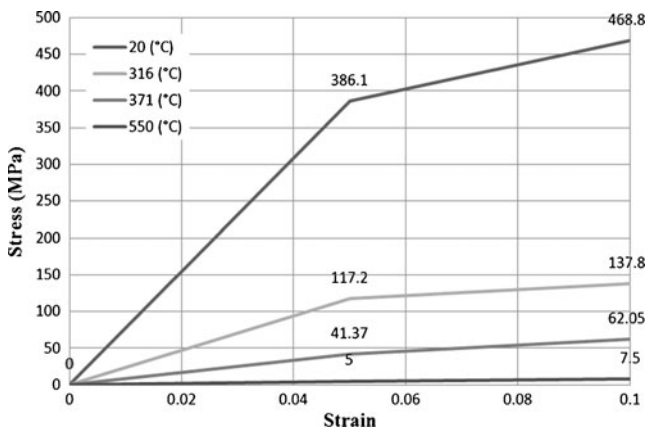


Fig. 5 Strain hardening of aluminum alloy 2519-T87 [29]

Another parameter that influences residual stress build up is electrode size. Effect of this parameter relates to the effect of molten pool size that electrode creates on the piece during welding. To study the effect of this parameter, 10 separate models with different molten pool sizes were designed whose molten pools sizes were 6.58, 6.20, 6.00, 5.73, 5.49, 4.77, 4.58, 4.39, 3.82 and 3.05 mm.

Material properties

The phase diagram for the base metal i.e. aluminum alloy 2519-T87 is shown in Fig. 3. [29] As temperature increases, material phase changes from  $\alpha+\theta$  to  $\alpha$  in 520°C. The next phase is  $\alpha+L$  at which point the material is melting. As material's phase changes from  $\alpha$  to  $\alpha+L$  very fast, first phase transfer is neglected with a good approximation in this study, but the second phase transition is modeled with the help of material library of ABAQUS elements. By including the user specified material annealing or melting temperature, when the material temperature exceeds it, ABAQUS would assume that the material at that point loses its hardening memory. The effect of prior work hardening is removed by

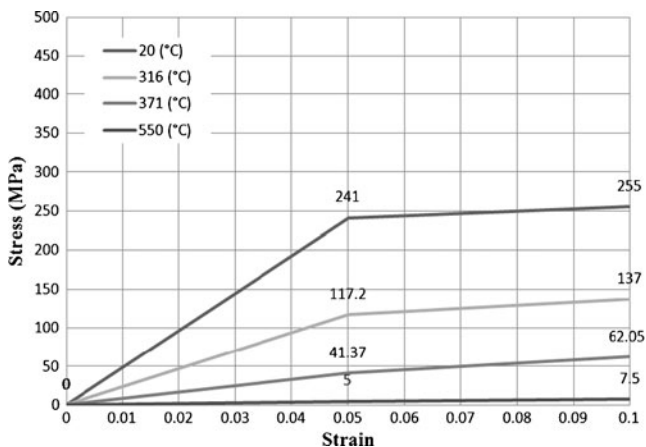


Fig. 6 Strain hardening of aluminum alloy 2319 [29]

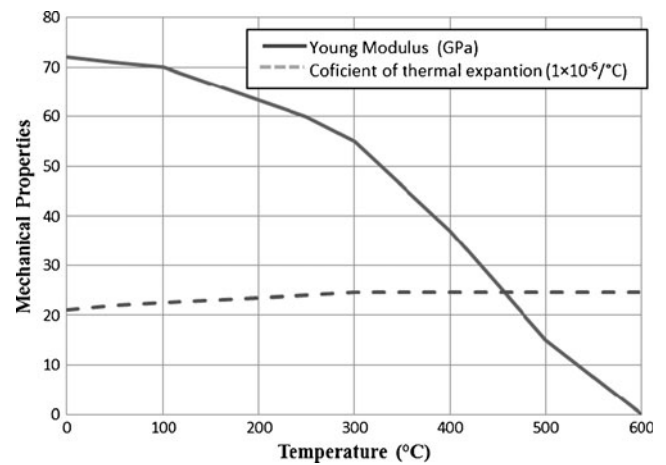


Fig. 7 Young's modulus and coefficient of thermal expansion of aluminum alloys 2519-T87 and 2319 as a function of temperature [29]

setting the equivalent plastic strain to zero. For kinematic and combined hardening models the back-stress tensor is also reset to zero. If the temperature of the material falls below the annealing temperature at a subsequent point in time, the material is allowed to work harden again. Therefore depending on the temperature history, a material may lose and accumulate memory several times which would simply correspond to repeated melting and re-solidification.

The material model has been used for this research is a plasticity model utilizing von Mises criterion with isotropic strain hardening. Due to the thermal loading and large strains which develop, a strain hardening model is more appropriate than an elastic-perfectly plastic model.

Yield stress of aluminum 2519-T87 and 2319 are plotted versus temperature in Fig. 4. The hardening curves used for Aluminum alloy 2519-T87 and 2319 are depicted in Figs. 5 and 6 respectively. The mass density of both materials is taken as 2823 Kg/m<sup>3</sup>. The melting temperature range for Al 2519-T87 is 555°C –668°C, and for Al 2319 is 543–643°C.

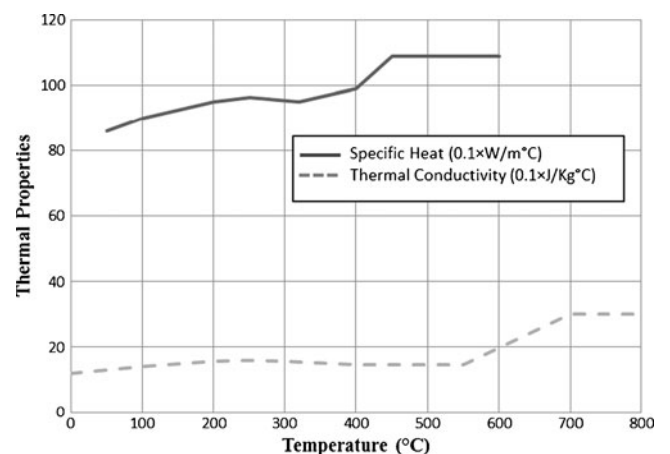
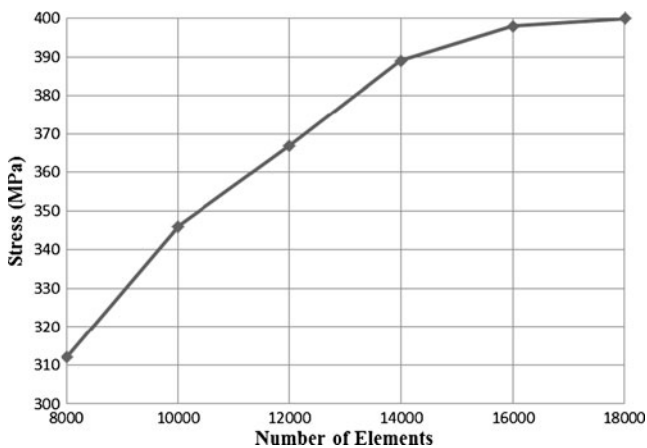


Fig. 8 Specific heat and thermal conductivity of aluminum alloys 2519-T87 and 2319 as a function of temperature [29]



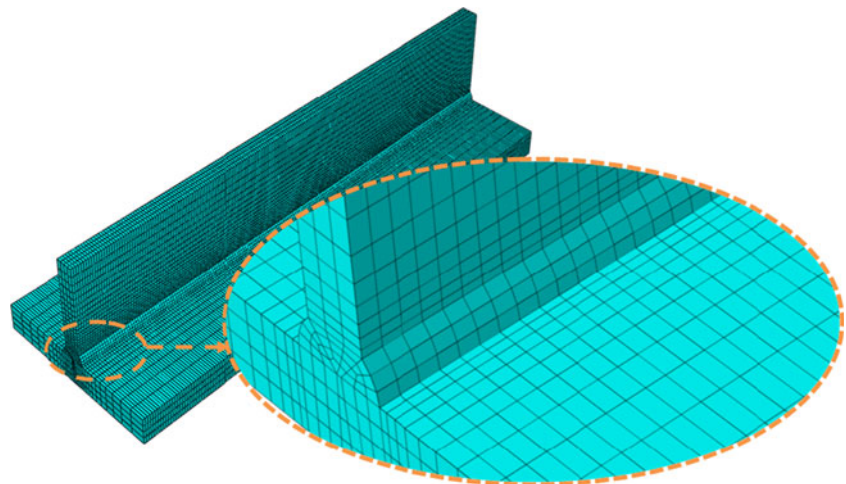
**Fig. 9** Convergence of maximum residual stress versus the number of elements used in the mesh

Due to lack of all required data for Al 2519 and Al 2319 and their similar chemical compositions, their data were used alternatively. Coefficients of thermal expansion and young's modulus are shown in Fig. 7, while thermal conductivity and specific heat as a function of temperature are shown in Fig. 8. The thermal effect caused by solidification of the welding pool was modeled by considering the latent heat of fusion, which was assumed to be 374 J/g [29].

#### Mesh and analysis method

Element C3D8T from ABAQUS is used which is an 8 node brick element that has the ability of being used in coupled thermo-structural analysis. Due to complicated material properties and nonlinear geometry and etc., welding process simulation is a tedious task which is also very sensitive to number of element used; so it is imperative that a minimum number of elements be chosen that are capable of producing acceptable results compared to experiments data. By increasing element number more than 18000 elements,

**Fig. 10** Tee joint finite element mesh



variation of maximum residual stress is negligible. Convergence trend of the results (maximum residual stress) obtained versus the choice of different number of elements used, is shown in Fig. 9 and their corresponding meshes are shown in Fig. 10.

A total number of 50 solution steps are enacted in ABAQUS to model element birth and heat source movement. In every step 3 elements are added to the model with initial temperature of 550°C based of melting temperature and heat source move 3 elements forward as shown in Fig. 11. Size of elements in welding direction is 1 mm so in each step heat source moves 3 mm forward. The inactive elements have no mechanical properties but possessing thermal properties same as the surrounding air.

Similarly 50 steps are included for the welding process with the final step done for cooling the model to the ambient temperature. To evaluate the effect of welding speed, three different speeds of 5, 6 and 7 mm/s are assumed for the various employed models. Different speeds are simply included by changing the time increment of each step.

Finally, quasi Newton method is used for the thermo-mechanical coupling analysis. When the stress analysis is dependent on the temperature distribution and the temperature distribution depends on the stress solution, coupled thermo-mechanical analysis is used. In ABAQUS the temperatures are integrated using a backward-difference scheme, and the nonlinear coupled system is solved using quasi-Newton's method. ABAQUS offers an exact as well as an approximate implementation of Newton's method for coupled temperature-displacement analysis.

#### Boundary conditions

A welding heat source is usually arc plasma radiating intense heat outwardly with decreasing temperature [25, 26], which the mathematical model of it can be represented by a Gaussian distribution.

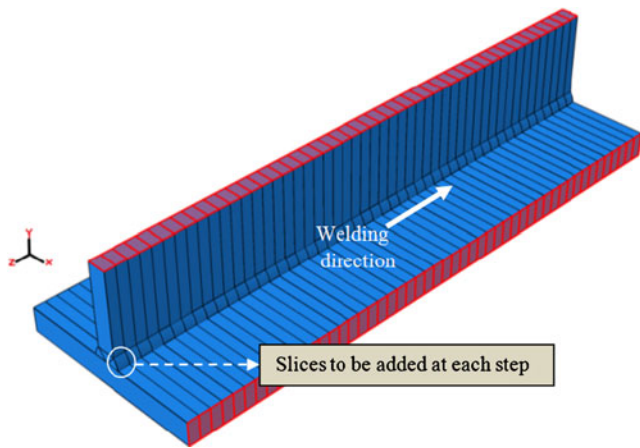


Fig. 11 Elements birth in the model

For modeling of the heat source, many authors [7, 12, 20], utilized the 3D double ellipsoid proposed by Goldak et al. [25]. The double ellipsoid geometry is used so that the size and shape of the heat source can be easily changed to model both the shallow penetration arc welding processes. The power or heat flux distribution is Gaussian along the longitudinal axis. The front half of the source is the quadrant of one ellipsoidal source while the rear half is the quadrant of another ellipsoidal source. Four characteristic lengths must be determined which physically correspond to the radial dimensions of the molten zone. If the cross-section of the molten zone is known from experiment, this information can be used to set the heat source dimensions. If precise data does not exist, Goldak et al. [25] suggest that is reasonable to take the distance in front of the source equal to one half the weld widths and the distance behind the source equal to two times the weld width. A double ellipsoidal heat source consists of two different concentric single ellipsoids suitable as a more advanced heat source as compared to the single ellipsoidal due to its greater flexibility in modeling shapes of moving heat sources realistically. Referring to Fig. 12, the heat

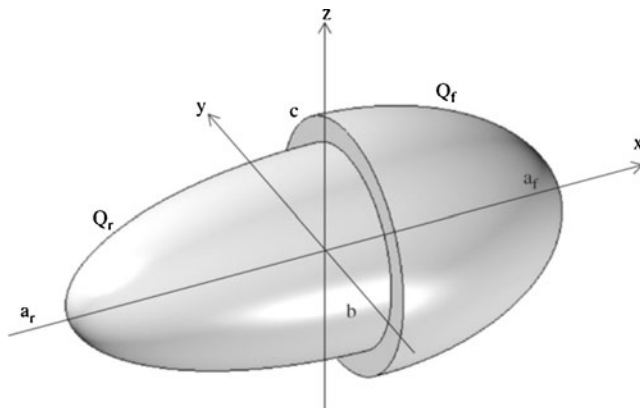


Fig. 12 Double ellipsoidal heat source model parameters

Table 2 Strain hardening of aluminum alloys 2519-T87 and 2319 [29]

a,mm	b,mm	C <sub>f</sub> ,mm	C <sub>b</sub> ,mm	f <sub>f</sub>	f <sub>r</sub>	n
30	30	24	82.6	0.45	1.55	85%

density at an arbitrary point (x, y, z) within each one-half ellipsoid is described by the following equations.

$$q_f = \frac{6\sqrt{3}Qf_f}{\pi\sqrt{\pi}c_fba} e^{-3\left(\frac{z^2}{a^2} + \frac{y^2}{b^2} + \frac{x^2}{c_f^2}\right)} \tag{1}$$

$$q_r = \frac{6\sqrt{3}Qf_r}{\pi\sqrt{\pi}c_bba} e^{-3\left(\frac{z^2}{a^2} + \frac{y^2}{b^2} + \frac{x^2}{c_b^2}\right)} \tag{2}$$

$$Q = \eta IV \tag{3}$$

$$f_f + f_r = 2 \tag{4}$$

In the above relations, x is the welding direction, a, b, c<sub>f</sub>, c<sub>b</sub> are the ellipsoidal heat source parameters, η is the efficiency, V and I are the arc voltage/current, and f<sub>f</sub>, f<sub>r</sub> are the proportional coefficients at the front and the back of the heat source. Since the heat source moves at a constant speed along a straight line, and the heat input Q from the source is constant, experience shows that such conditions lead to a fused zone of constant width. Moreover, zones of temperatures below the melting point also remain at constant width [31]. The heat source parameters that used in this study are given in Table 2.

To study the effects of voltage/current on residual stresses three heat inputs are created in different models such that the heat inputs be equal to 11.5, 8.625, 5.25 KW. Assuming a transient solution for the convection, heat transfer in the surrounding temperature of 20°C gives the coefficient of convection as a function of temperature for Aluminum 2519-T87 and 2319 as shown in Fig. 13. The

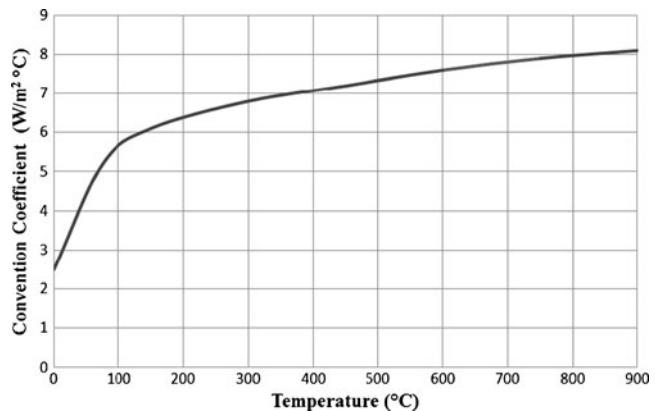
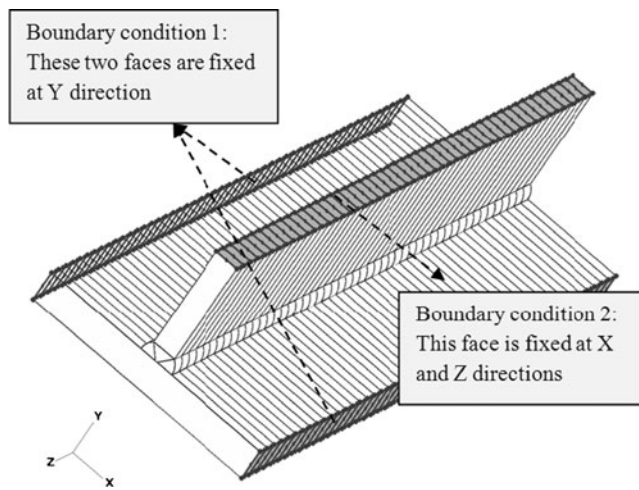


Fig. 13 Convection coefficient of aluminum alloys 2519-T87 and 2319 as a function of temperature [29]



**Fig. 14** Boundary condition for different steps of solution procedure

radiation effects are neglected since they are typically much smaller than the convection effects. In the first 50 steps of welding process boundary conditions 1 and 2 are assumed, and in the final step (cooling) only boundary condition 2 is assumed while condition 1 is relaxed; these boundary condition are shown in Fig. 14.

**Results and discussion**

The simulation was run for a time period of 68700 s, i.e., more than 19 h, allowing for the complete thermo-structural cycle, including heating and subsequent air cooling to take place. The temperature profiles obtained at 25 s is shown in Fig. 15. Figure 16 shows temperature history measured by the thermocouple and also evaluated by finite element analysis. The welding condition for Fig. 16 is:

Welding speed: 6 mm/s, heat input: 11.5 KW, Thickness: 10 mm, Molten pool size: 6 mm.

**Fig. 15** Temperature contours of the model at t=25 s

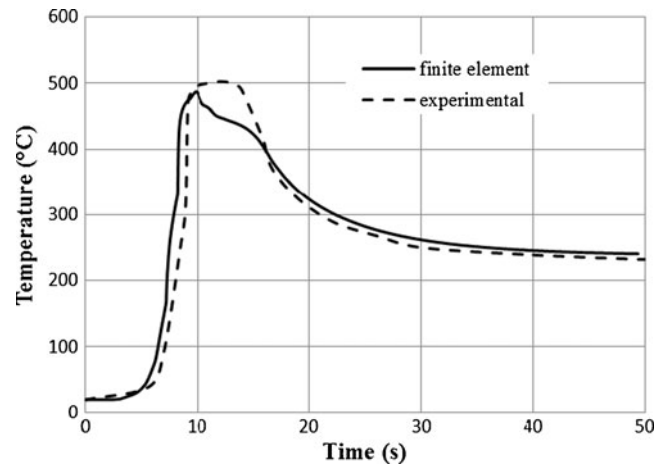
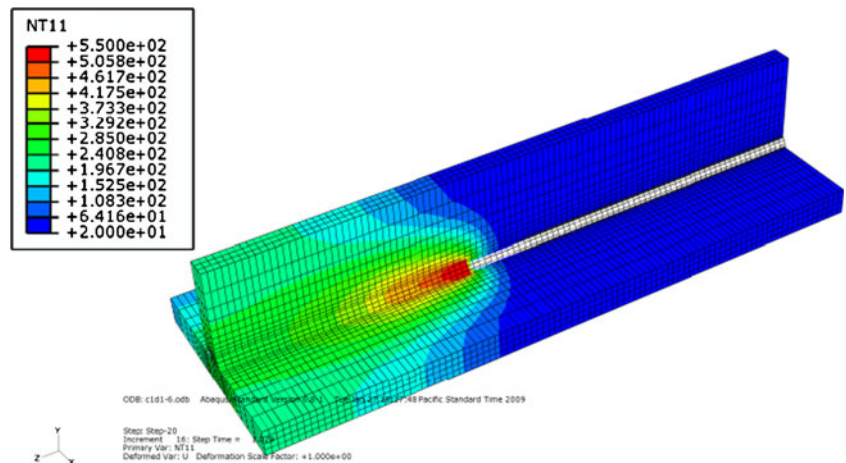


**Fig. 16** Temperature variation by time for finite element and experiment

It shows that the thermal analysis is sufficiently accurate and finite element model gives good results for temperature distribution, and that neglected radiation heat transfer seems to be a reasonable assumption. The difference between experiment and simulation result is caused by rapid evaluations of temperatures that cannot have been registered by the thermocouple due to its thermal inertia and thermal resistance phenomena. In accordance to the temperature diagrams, temperature in the parts increases to 550°C in the welding direction. Figure 17 shows the temperature history of some points from beginning to middle of welding direction (molten pool center). Except two first points other points seem to have the same temperature history which suggests the heat transfer rate can be assumed as a steady state process in a short time after the welding is started.

Figure 18 shows Von Mises residual stress contours after welding is completed. It shows that the maximum stress occurs at the center of the molten pool zone since thermal strains in this zone have increased intensively with solidifica-

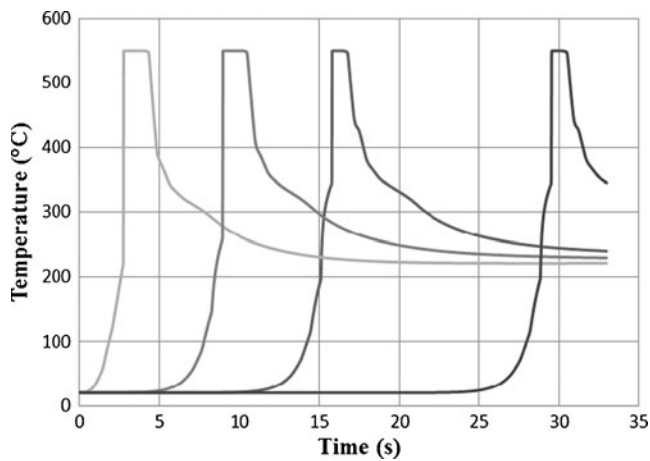


**Fig. 17** Temperature history for some points in welding direction

tion. Stresses at physical boundary zones are not significant since the boundary conditions are selected to allow free movement there. The dominant tensile stresses occur in the Z direction, e.g. S33 component which emphasizes that the probability of crack growth normal to Z direction is more than other directions (S33 is principal stress in the Z direction). Figure 19 shows a comparison of experimental and finite element results. It also shows that the finite element results exhibit good agreement with experimental ones on positions of strain gauges. The differences between these results are possibly due to ignoring phase change from  $\alpha+\beta$  to  $\alpha$  at the start, and/or the measurement and/or truncation errors in numerical analysis at the end.

The FEA results show that the longitudinal high tensile residual stresses occur in the region near the weld line and drop in value when moving away up to the middle of the plate, but near the boundaries the residual stresses increase again. The analysis results also show that the transverse and normal stresses are small in magnitude (nearing zero) in the

region close to the centre line, and tend to increase towards the outer edges of the plate, in agreement with experimental results (Fig. 19).

Residual stresses are produced by an uneven distribution of nonelastic strains including Plastic and thermal strains. Large local plastic strains in the solidified weld metal and the heat affected zone originate from the very non-uniform temperature field around the weld pool [4]. During the welding thermal cycle, complex transient thermal stresses are produced in the weldment and the surrounding joint. Beneath the welding arc, stresses are close to zero because molten metal does not support shear loading. As the expansion of metal surrounding the weld pool is restrained by the base metal, stresses become compressive adjacent to the welding arc and moving away from the welding arc. These compressive stresses are as high as the yield strength of the base metal at corresponding temperatures. The temperatures of the metal surrounding the weld pool are very high and therefore cause the yield strength of the material to become quite low [32].

Stresses occurring in regions farther away from the welding arc are tensile and balance with these compressive stresses near the weld pool. As the weld-metal and base metal regions cool and shrink the regions in and adjacent to the weld, experience tensile stresses. As the distance from the weld increases, the stresses become compressive. High tensile residual stresses in areas near the weld can cause premature failures of welded structures under certain conditions. Compressive residual stresses in the base plate can reduce the buckling strength of a structural member subjected to compressive loading [32].

To study the relative effects of input parameters on the residual stresses, a total of 84 finite element models with combinations of different input parameters are tested as depicted schematically in Fig. 20. Three welding speeds,

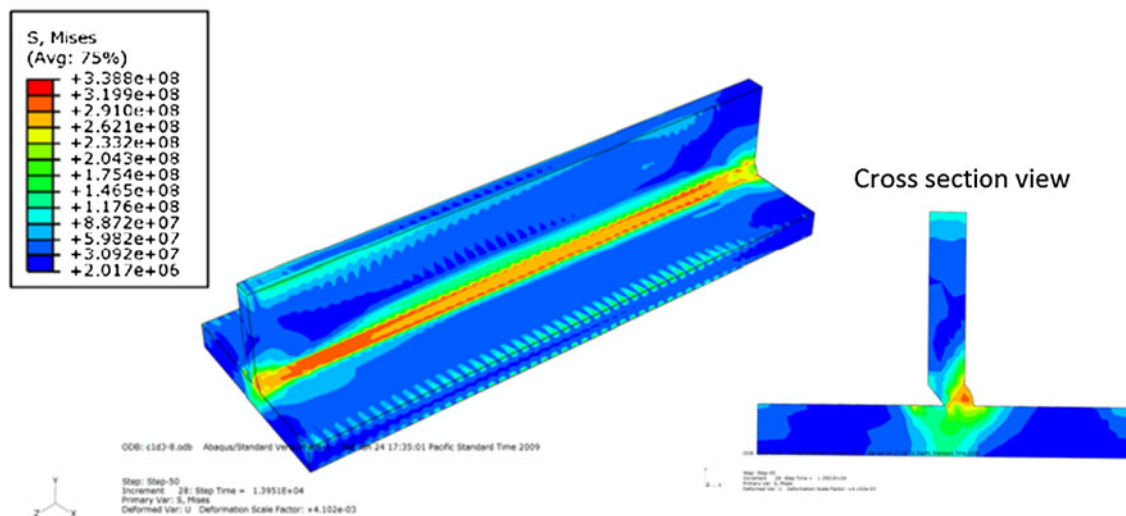
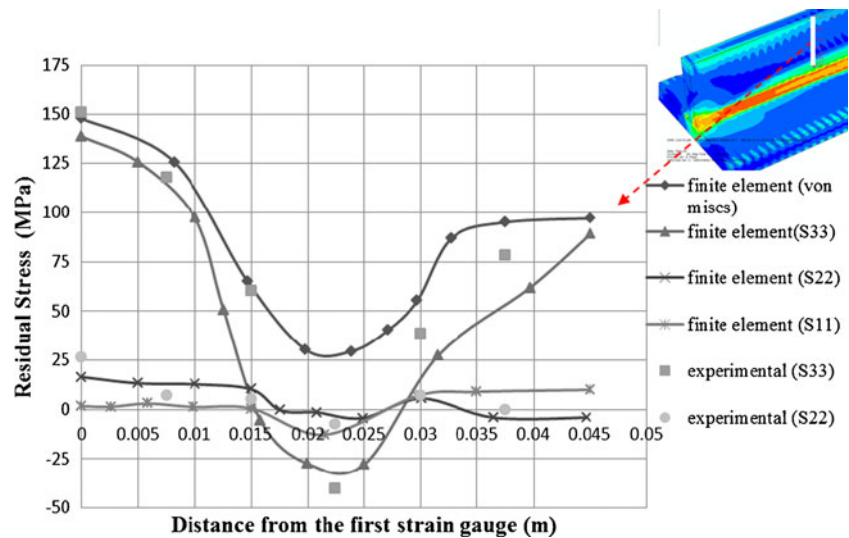


**Fig. 18** Residual stress contours after welding



**Fig. 19** Residual stresses measured by experimental and finite element methods



ten electrode sizes, three voltage/current (heat input) values, and three plate thicknesses are chosen in combination with one another. Figure 21(a), (b), and (c) show maximum residual stresses as a function of heat input (voltage/current) for different electrode sizes, plate thicknesses and welding speeds of: 7, 6, and 5 (mm/s) respectively. The residual stresses due to welding of an aluminum tee joint of 2519 alloy with given different welding parameters can be obtained from charts 21-(a), 21-(b), and 21-(c). Furthermore, for tee joint welding of plates of different thicknesses the best combination of welding parameters (electrode size, welding current/voltage and welding speed) for minimum residual stresses also can be selected from those charts.

**Effect of welding speed**

Case C-1 in Table 3 is designed to study the effect of welding speed on residual stresses. Results of longitudinal and transverse residual stresses for case C-1 are plotted along gage line 1, as a function of the distance from the center of weld bead (see Fig. 2), and are shown in Fig. 22(a) and (b) respectively. Higher welding speeds have beneficial effect in reducing residual stresses. Low welding speeds result in

high heat input per unit length of the weld, producing relatively larger weld puddle and HAZ (heat affected zone) causing an increase in residual stresses in the plates around the welding line; thus closer to the weld centerline, lower welding speeds cause higher tensile stresses. Further away from the HAZ the stress profile remains less affected by any changes in the welding speed.

**Effect of voltage/current**

Case C-2 in Table 3 is designed to study the effect of current/voltage on residual stresses. Results of longitudinal and transverse residual stresses for case C-2 are plotted along gage line 1, as a function of the distance from the center of weld bead (see Fig. 2), and are shown in Fig. 23(a) and (b) respectively. The change in heat input per unit length of welding is directly proportional to the change in the welding current/voltage (see Eq. 3) provided the other welding parameters are kept unchanged. It is observed that welding current/voltage has opposite effect compared to welding speed.

The effect of welding speed on residual stress is higher than the effect of current/voltage as shown in Figs. 22(a), (b), 23(a), and (b). Welding current/voltage has a direct algebraic relation to the heat input of weldment (see Eq. 3); while welding speed has an exponential relation to the heat input of weldment (see Eq. 1).

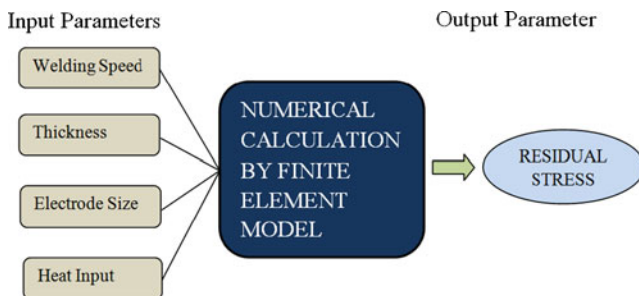


**Fig. 20** Schematic flow of input parameters for the finite element model

**Effect of thickness**

Case-3 in Table 3 is designed to study the effect of thickness on residual stresses. Results of longitudinal and transverse residual stresses for case C-3 are plotted along gage line 1, as a function of the distance from the center of weld bead (see Fig. 2), and are shown in Fig. 24(a) and (b) respectively. Strength of the plate and the heat flow function are dependent upon the thickness whereby increasing it would

**Fig. 21** Maximum residual stresses as a function of heat input for different electrode (molten pool) size and thickness: **a** 7 mm/s welding speed **b** 6 mm/s welding speed **c** 5 mm/s welding speed

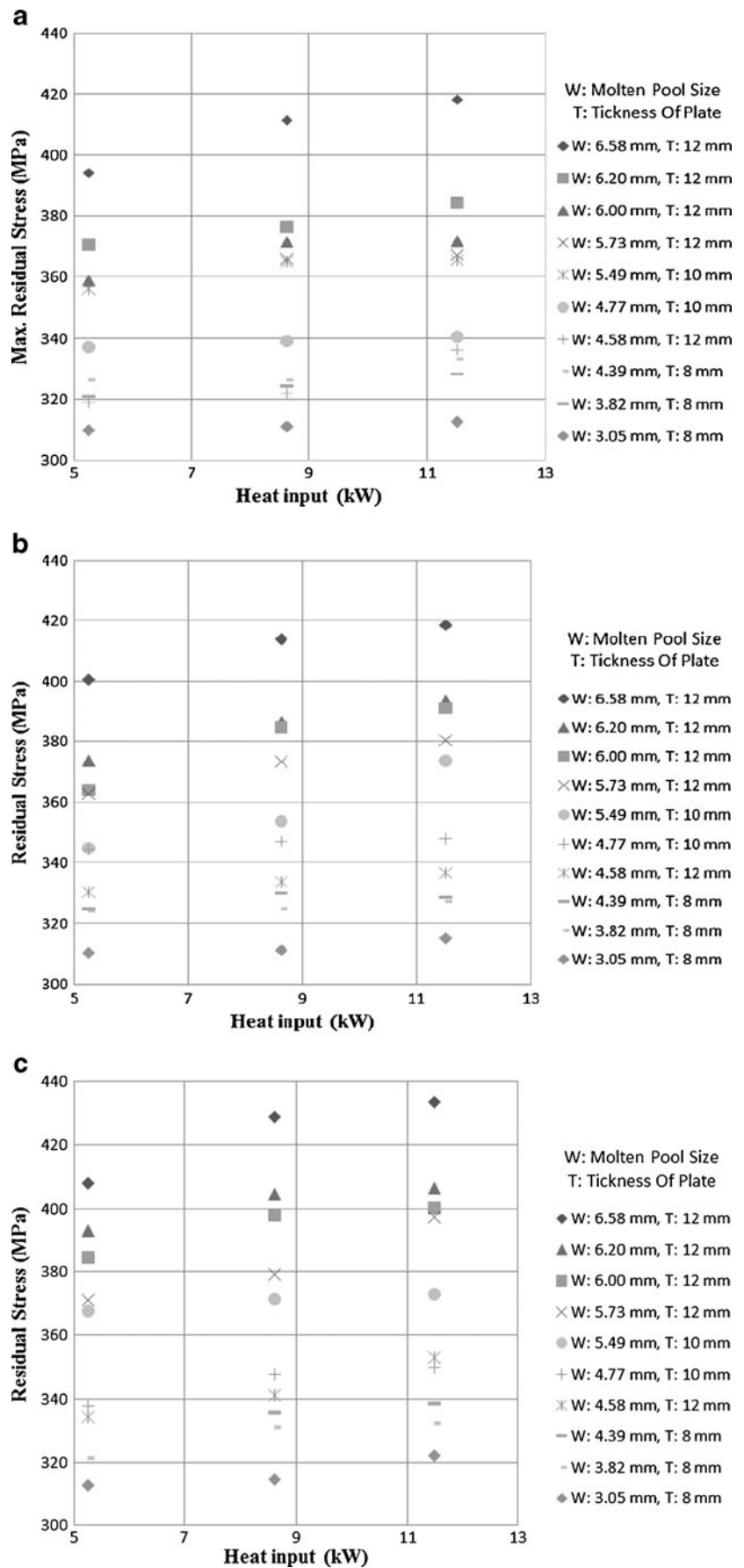


**Table 3** Cases designed to study the effect of geometry and other welding parameters on residual stress build up

Case	Model	Welding speed (mm/s)	Heat input (kW)	Molten pool size (mm)	Thickness (mm)
Effect of welding speed	C-1	5, 6, 7	11.5	6.00	12
Effect of voltage/current	C-2	6	5.25, 8.625, 11.5	6.00	12
Effect of plate thickness	C-3	6	11.5	6.00	8, 10, 12
Effect of electrode size	C-4	6	11.5	6.58, 6.20, 6.00	12

increase the strength and change the heat flow, causing the thermal strains to drop off with reduction of plastic areas which consequently lead to a decrease in residual stresses. The effect of thickness on residual stresses near the welding line are little different from those located far from it, since an

increase in the thickness causes the strength of whole model to increase. The effect of thickness on the residual stress variations between points near and far from the center of welding line is due to its effect on the heat flow affected by it. The effect of thickness on residual stress change is more

**Fig. 22** Effect of welding speed on residual stresses in welding line: **a** Longitudinal residual stress **b** Transverse residual stress

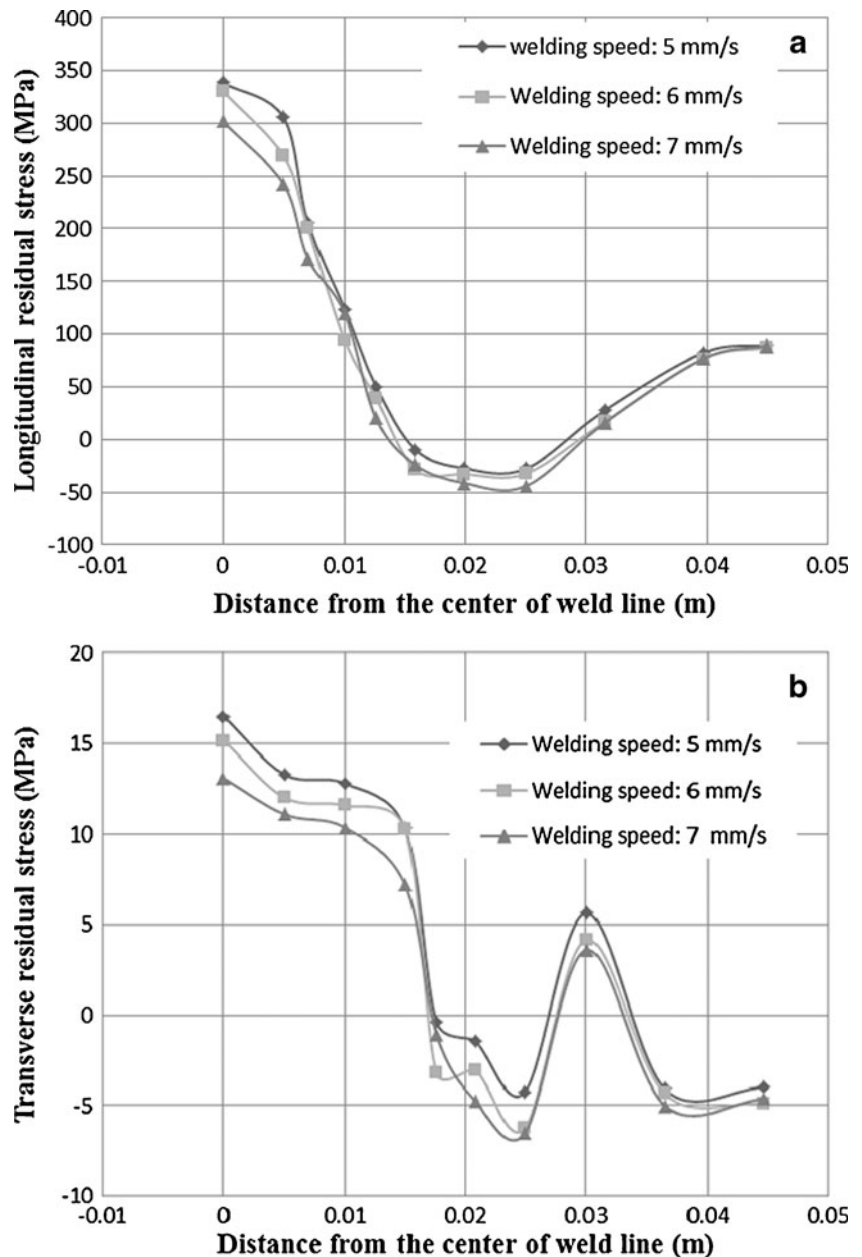
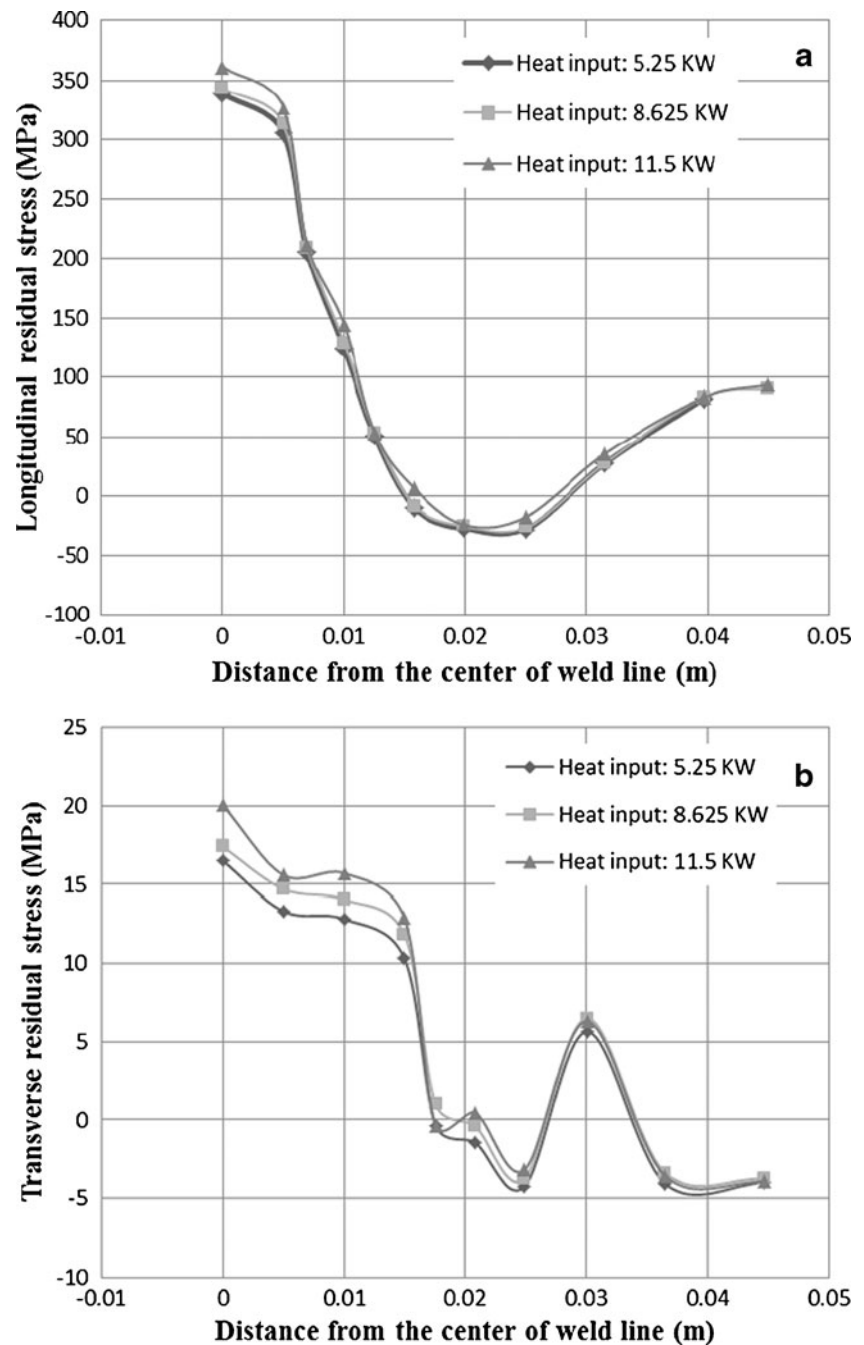


**Fig. 23** Effect of welding current or voltage (heat input) on residual stresses in welding line: **a** Longitudinal residual stress. **b** Transverse residual stress



than welding current but is less than welding speed as can be concluded from the presented figures.

#### Effect of electrode sizes

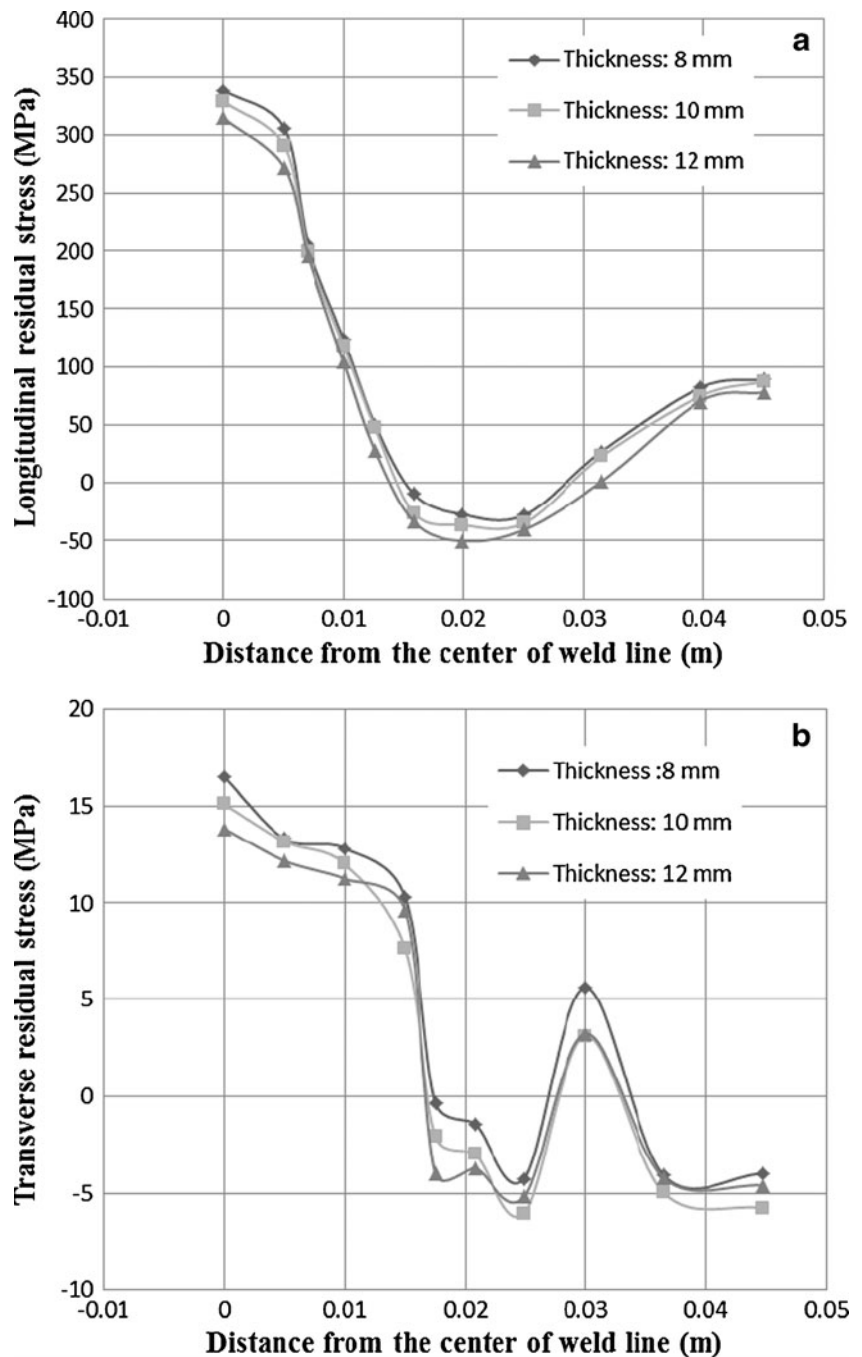
Case-4 in Table 3 is designed to study the effect of electrode size on residual stresses.

Results of longitudinal and transverse residual stresses for case C-4 are plotted along gage line 1, as a function of the distance from the center of weld bead (see Fig. 2), and are shown in Fig. 25(a) and (b) respectively. Decreasing the

electrode size causes a decrease in the heat input to the plates and the size of the molten pool, which causes a reduction in the residual stresses. The effect of electrode size around the welding line is more than the outlying areas of the welding zone. So near the welding line an increase in the electrode size, results in an increase of molten pool size and HAZ as well as the amount of heat input, as the most significant parameters causing an increase in residual stresses.

The sensitivity of residual stress to electrode size is more than other parameters as shown in the presented figures. This is because of electrode size influencing both the

**Fig. 24** Effect of thickness on residual stresses in welding line:  
**a** Longitudinal residual stress **b** Transverse residual stress



molten pool size and heat input to the plate; thus by increasing the electrode size for a fixed body heat flux the amount of heat input per unit length of plates increases, followed by an increase of HAZ zone and finally leading to the residual stress increases.

**Conclusions**

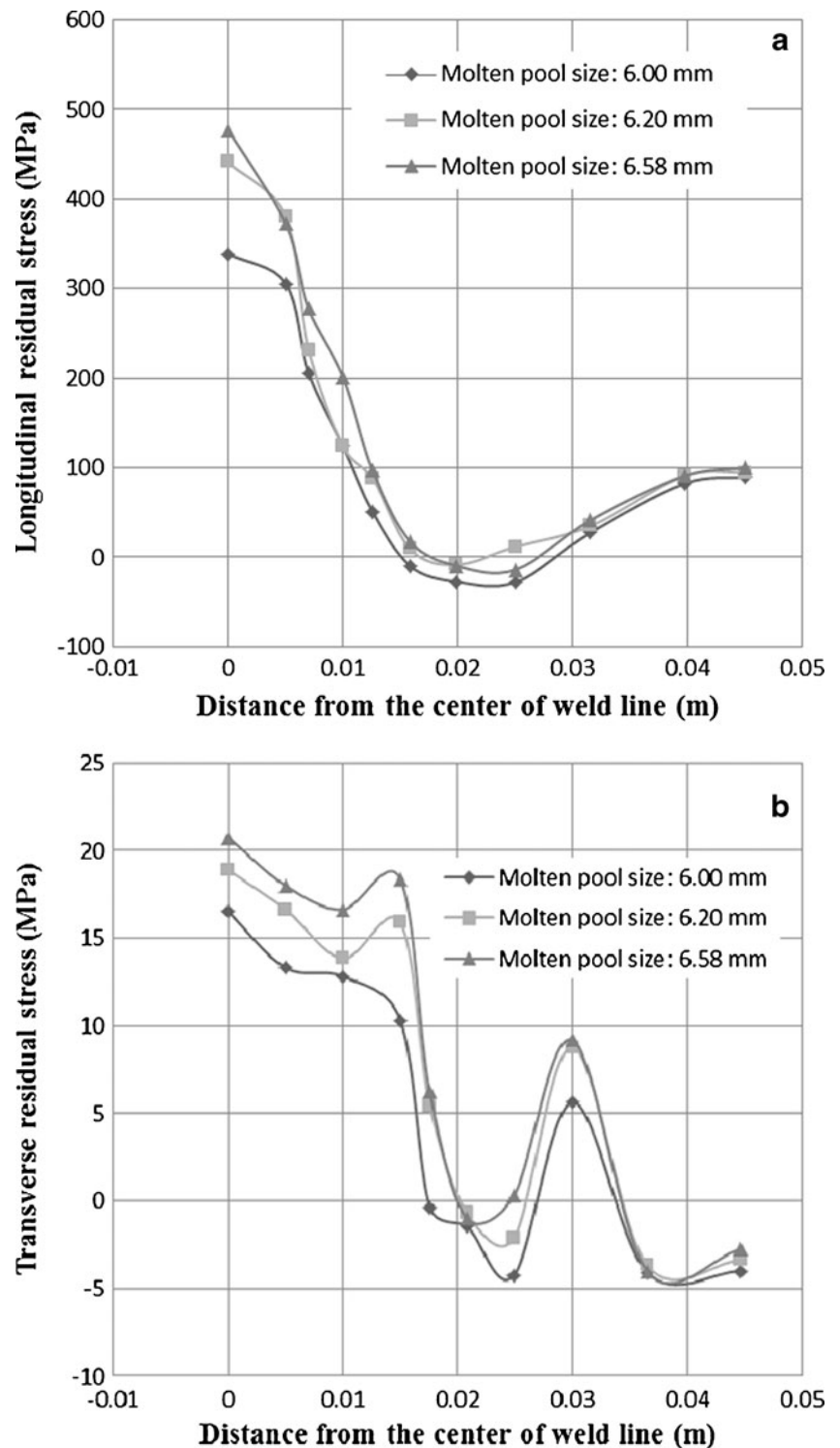
A three-dimensional numerical model has been developed to simulate the gas arc welding process of tee joints,

considering all the important physical mechanisms of the welding process during both heating and cooling except one phase transition and Metallurgical aspects stages.

This research effort was successful in determining the weld heat affected zone and resulting final residual stress state for a tee section joint using finite element simulations. Temperature history and residual stresses that are evaluated by finite element analysis for different location on the plate piece are close to the experimental results.

The effect of geometrical and other welding parameters on stress magnitudes and distribution are evaluated for the

**Fig. 25** Effect of electrode size on residual stress in welding line: **a** Longitudinal residual stress **b** Transverse residual stress



thin plates (thick plates needs multi pass welding) used for the weldment. Based on the results presented, the following points can be concluded:

1. Neglecting the radiation heat proved to be an acceptable assumption not influencing the results especially far from the welding line.
2. Higher welding speed and thickness have a decreasing effect on the magnitude of the residual stresses and the extent of the affected zone, but electrode size and current/voltage have an increasing influence on the residual stresses.
3. The relative sensitivity of residual stresses to the electrode size is more than other parameters. Effect of

welding speed in changing residual stress is more than the welding current/voltage and thickness. The welding current/voltage has less influence on residual stress than other parameters.

- Using the charts that are presented, the residual stress of welding a tee joint made of aluminum 2519-T87 with different welding parameters can be obtained. It could be used to provide the best combination of parameters' choices for minimum residual stresses.

## References

- Zhang J, Dong P, Brust F (1999) Residual stress analysis and fracture assessment of weld joints in moment frames. *ASME PVP—Fracture, Fatigue and Weld Residual Stress*. 393 201–207
- Preston R, Smith S, Shercliff H, Withers P (1999) An investigation into the residual stresses in an aluminum 2024 test weld. *ASME PVP—Fracture, Fatigue and Weld Residual Stress*. 393 265–277
- Dong P, Hong J, Bynum J, Rogers P (1997) Analysis of residual stresses in Al-Li alloy repair welds. *ASME PVP—Approximate Methods in the Design and Analysis of Pressure Vessels and Piping Components*. 347 61–75
- Karlsson RI, Josefson BL (1990) Three-dimensional finite element analysis of temperatures and stresses in a single-pass butt-welded pipe. *ASME Journal of Pressure Vessel Technology* 112:76–84
- Chao Y, Qi X (1999) Thermo-mechanical modeling of residual stress and distortion during welding process. *ASME PVP—Fracture, Fatigue and Weld Residual Stress*. 393 209–213
- Oddy A, Goldak S, McDill JA (1989) Transformation plasticity and residual stresses in single-pass repair welds. *ASME PVP—Weld Residual Stresses and Plastic Deformation*. 173 13–18
- Michaleris P, Feng Z, Campbell G (1997) Evaluation of 2D and 3D FEA models for predicting residual stress and distortion. *ASME PVP—Approximate Methods in the Design and Analysis of Pressure Vessels and Piping Components*. 347 91–102
- Michaleris P, Dantzig J, Tortorelli D (1999) Minimization of welding residual stress and distortion in large structures. *Welding Journal, Welding Research Supplement* 361–366
- Tsai CL, Park SC, Cheng WT (1999) Welding distortion of a thin-plate panel structure. *Welding Journal, Welding Research Supplement* 156–165
- McDill JMJ, Oddy AS, Goldak JA (1993) Comparing 2-D plane strain and 3-D analyses of residual stresses in welds. *International Trends in Welding Science and Technology, Proceedings of the 3rd International Conference on Trends in Welding Research*, ASM International, Materials Park, OH. pp 105–108
- Hong JK, Tsai CL, Dong P (1998) Assessment of numerical procedures for residual stress analysis of multipass welds. *Welding Journal, Welding Research Supplement*, pp 372–382
- Goldak J, Chakravarti A, Bibby M (1984) A new finite element model for welding heat sources. *Metallurgical Transactions B*, pp 299–305
- Junek L, Slovacek M, Magula V, Ochodek V (1999) Residual stress simulation incorporating weld HAZ microstructure. *ASME PVP—Fracture, Fatigue and Weld Residual Stress*, pp 179–192
- Vincent Y, Jullien JF, Cavallo N, Taleb L, Cano V, Taheri S, Gilles Ph (1999) On the validation of the models related to the prevision of the HAZ behaviour. *ASME PVP Fracture, Fatigue and Weld Residual Stress*, pp 193–200
- Brown S, Song H (1992) Finite element simulation of welding of large structures. *ASME Journal of Engineering for Industry*, pp 441–451
- Dubois D, Devaux J, Leblond JB (1984) Numerical simulation of a welding operation: calculation of residual stresses and hydrogen diffusion. *ASME Fifth International Conference on Pressure Vessel Technology, Materials and Manufacturing*, San Francisco, pp 1210–1238
- Goldak J, Gu M (1995) Computational weld mechanics of the steady state. *Mathematical modelling of weld phenomena 2*, The Institute of Materials, London, 207–5
- Oddy AS, McDill JMJ, Goldak JA (1990) Consistent strain fields in 3D finite element analysis of welds. *ASME Journal of Pressure Vessel Technology, Technical Briefs*, pp 309–311
- Dong P, Ghadiali PN, Brust FW (1998) Residual stress analysis of a multi-pass girth weld. *ASME PVP—Fatigue, Fracture, and Residual Stresses*, pp 421–431
- Feng Z, Wang XL, Spooner S, Goodwin GM, Maziasz PJ, Hubbard CR, Zacharia T (1996) A finite element model for residual stress in repair welds. *ASME PVP Residual Stresses in Design, Fabrication, Assessment and Repair*, pp 119–125
- Karlsson L, Jonsson M, Lindgren LE, Nasstrom M, Troive L (1989) Residual stresses and deformations in a welded thin-walled pipe. *ASME PVP—Weld Residual Stress and Plastic Deformation*, pp 7–10
- Grong O, Myhr OR (1993) Modelling of the strength distribution in the heat affected zone of 6082-T6 aluminum weldments. *Mathematical Modelling of Weld Phenomena*, The Institute of Materials, London, pp 300–311
- ESI Group, 2000, SYSTUS 2000 Analysis reference manuals, ESI North America, 13399 West Star, Shelby Township, MI
- Chan B, Pacey J, Bibby M (1999) Modeling gas metal arc weld geometry using artificial neural network technology. *Can Metall Quart*, pp 43–51
- Goldak J, Chakravarti A, Bibby M (1984) A new finite element model for welding heat sources. *Metallurgical Transactions B*, pp 299–305
- Goldak J, Chakravarti A, Bibby M (1985) A double ellipsoidal finite element model for welding heat sources. In: *IIW Doc. No. 212-603-85*
- Rybicki EF, McGuire PA, Merrick E, Wert J (1982) The effect of pipe thickness on residual stresses due to girth welds. *ASME Journal of Pressure Vessel Technology*, pp 204
- Fricke S, Keim E, Schmidt J (2001) Numerical weld modeling—a method for calculating weld-induced residual stresses. *Nucl Eng Des* 206:139–150
- Michaleris P, Feng Z, Campbell G (1997) Evaluation of 2D and 3D FEA models for predicting residual stress and distortion. *ASME PVP—Approximate Methods in the Design and Analysis of Pressure Vessels and Piping Components*, 347, pp 91–102
- Callister W (1995) *Materials science and engineering*. John Wiley & Sons, Inc., New York, NY, pp.236–243, 142, 558, 560
- ESI Group (2000) SYSTUS 2000 analysis reference manuals, ESI North America, 13399 West Star, Shelby Township, MI
- Masubuchi K (1980) *Analysis of welded structures-residual stress, distortion, and their consequence*. Pergamon, New York, p 205